REVIEW

doi:10.1038/nature19948

Unravelling biological macromolecules with cryo–electron microscopy

Rafael Fernandez-Leiro[1]* & Sjors H. W. Scheres[1]*

Knowledge of the three-dimensional structures of proteins and other biological macromolecules often aids understanding of how they perform complicated tasks in the cell. Because many such tasks involve the cleavage or formation of chemical bonds, structural characterization at the atomic level is most useful. Developments in the electron microscopy of frozen hydrated samples (cryo–electron microscopy) are providing unprecedented opportunities for the structural characterization of biological macromolecules. This is resulting in a wave of information about processes in the cell that were impossible to characterize with existing techniques in structural biology.

Biological macromolecules adopt complicated three-dimensional (3D) structures that are crucial to their function. Some macromolecules, such as enzymes, act alone to provide chemical environments that favour the catalysis of specific chemical reactions. Other macromolecules form larger complexes with protein partners, nucleic acids, lipids or sugar molecules. Many such complexes perform their functions through the relative movements of individual parts, in a way that resembles how man-made machines work[1]. A fundamental goal of modern biology is to understand how these complicated structures perform their tasks.

Macromolecular complexes are too small to be seen with visible light. Photons with wavelengths that are short enough to visualize details at the atomic level are found in the X-ray region of the electromagnetic spectrum. X-rays interact weakly with biological matter, which makes it difficult to use them to study individual protein complexes. But when many copies of the same protein are arranged into a 3D crystal, information about the atomic structure of the protein can be obtained through X-ray diffraction experiments. This technique, known as X-ray crystallography, has been the most important tool in structural biology for more than two decades (Fig. 1). Another technique that is used to characterize the structures of proteins is nuclear magnetic resonance (NMR) spectroscopy, which measures distance-dependent interactions between atoms. NMR can be used to infer the structure of relatively small proteins, and it provides unique information about the dynamics of proteins and their interactions with other molecules.

Electrons can also be used to look at protein structures. Proteins scatter electrons about ten-thousand times more strongly than they do X-rays, and electrons can be accelerated by electric fields of several hundreds of thousands of volts to wavelengths that are much shorter than the distances between the atoms in protein structures. Moreover, the electric charge of electrons makes it relatively easy to focus them with electromagnetic lenses. Microscopes can therefore be built that use electrons to make images with atomic-level detail. The contributions of electron microscopy to structural biology have been modest in comparison with X-ray crystallography and NMR, but present trends indicate that this is changing (Fig. 1). In 2016, the one-thousandth atomic structure derived from electron microscopy images[2] was entered into the Protein Data Bank (PDB), the main repository for protein structures. In this Review, we describe how images from an electron microscope can be used to study the structures of proteins and how rapid progress in structure determination through electron microscopy in the past few years has been heralded as the start of a revolution in structural biology[3]. We also highlight how the unique characteristics of this technique have already changed structural biology and identify opportunities through which electron microscopy will continue to transform understanding of how macromolecules perform intricate tasks in the cell.

Cryo–electron microscopy

Because electrons are scattered by molecules in the air, electron microscopes must be operated in a high vacuum. This poses a problem when studying biological samples, most of which occur naturally in an aqueous environment. Biological structures are also sensitive to radiation damage. For each electron that contributes to the formation of an image, there will be three electrons that deposit energy in the sample. This energy causes the cleavage of chemical bonds and ultimately destroys the structures of interest. By keeping samples at cryogenic temperatures, cryo-electron microscopy (cryo-EM) enables their preservation in a high vacuum and provides them with some protection against the effects of radiation damage[4].

The placement of a cryo-EM sample inside an electron microscope is shown in Box 1. To prepare the sample, a few microlitres of a purified protein solution is applied to a metal (usually copper) grid, on top of which lies a thin film of amorphous carbon that contains holes. After any excess liquid is blotted with filter paper, the grid is plunged into liquid ethane[5]. Ideally, this results in the formation of a thin layer of non-crystalline or vitreous ice, in which copies of the protein are deposited in a range of orientations. Images that are captured through the holes in the carbon film contain two-dimensional (2D) projections of individual protein complexes, which are called particles. Projections of particles in various orientations provide complementary information about the underlying 3D object. Numerous 2D projections can therefore be combined into a single 3D reconstruction, provided that their relative orientations are known. Unfortunately, this information is lost in the experiment because the individual particles tumble randomly in solution before the sample is vitrified.

The relative orientations of individual particles can still be determined a posteriori by processing the 2D projection images using a computer[6], a process known as single-particle analysis. Images

[1]MRC Laboratory of Molecular Biology, Cambridge Biomedical Campus, Cambridge CB2 0QH, UK. *These authors contributed equally to this work.

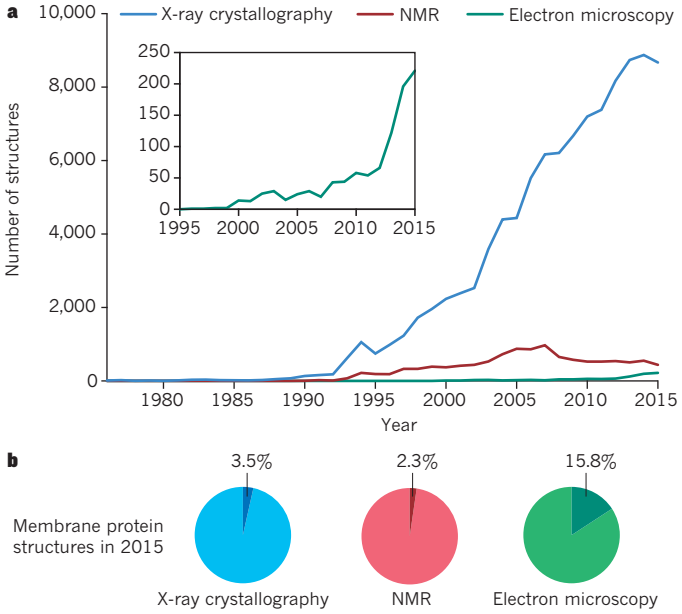

Figure 1 | Growth in structural biology over the past 40 years. **a**, The number of structures recorded in the PDB, as determined by the techniques of X-ray crystallography (blue), NMR (red) and electron microscopy (green) between 1975 and 2015. The number of structures that were determined by electron microscopy between 1995 and 2015 is also shown (inset), which highlights the recent growth in structure determination using this method. **b**, The percentage of membrane protein structures discovered in 2015 using each of the three techniques.

collected with single-particle cryo-EM are of low contrast because the proteins scatter electrons only about 30% more than does the surrounding ice. This would not be a problem if many electrons could be used to determine small differences in image intensities. However, to reduce the effects of radiation damage, the number of electrons used must be carefully limited, resulting in extremely noisy images. Such noise impedes the accurate assignment of orientation to the particles, which becomes the main bottleneck.

Progress in cryo-EM

Larger protein complexes and complexes that contain oligonucleotides give rise to images with higher signal-to-noise ratios. The presence of internal symmetry in a complex also helps to improve the resolution. This explains why the structures of ribosomes and icosahedral virus capsids have long been at the forefront of the cryo-EM field. By 2008, the structures of several viruses had been solved to near-atomic resolution[7–9]. Ribosome structures could also be calculated to a resolution of 6 Å (refs 10–12). These successes built on important developments in instrumentation, experimental procedures and image processing in the preceding 40 years[13–15]. And in the past 5 years, a number of developments have further changed the scope of cryo-EM-based structure determination.

By 2010, the quality of available cryo-EM protein structures did not support theoretical considerations about radiation damage, which predicted that structure determination should be possible to atomic resolution for protein complexes with molecular weights as low as 100 kDa (ref. 16). The difference could be explained in part by the inefficient detection of electrons. Images were originally recorded on photographic film, but in the early 2000s, the development of cameras containing a digital charge-coupled device (CCD)[17] opened the path to higher throughput and automated data acquisition[18]. Photographic film detects only about one-third of the incoming electrons. CCDs are even less efficient, however, because an extra conversion from electrons to photons leads to an overall detection rate of less than one-fifth of the incoming electrons[19]. This affects cryo-EM-based structure determination exactly at its bottleneck: the low number of electrons that is used to limit radiation damage results in images that are too noisy to determine reliably the orientation of particles.

Three companies had produced prototypes of a new generation of digital electron detectors by 2012. The innovative chips were sufficiently resistant to radiation damage to enable the direct detection of electrons, which improved the efficiency of detection to around half of the incoming electrons[20]. Moreover, the modernized electronics that surround these direct electron detectors facilitated fast image capture, much like the burst mode of contemporary photographic cameras. Counting individual electron events on the fastest camera available led to an even better efficiency of electron detection[21]. Fast image capture also addressed a problem that is associated with frozen hydrated samples: energy released by the incoming electrons causes movement inside the ice layer, which blurs the resulting images. Movies recorded during exposure of the sample to electrons could be processed to effectively remove the blurring effects[22,23], which facilitated structure determination to an unprecedented resolution from far fewer data than before[21,24].

Meanwhile, another main impediment to high-resolution cryo-EM-based structure determination had been solved. Many macromolecular machines adopt a range of conformations in solution, and the purification or formation of these protein complexes is seldom perfect. This means that samples prepared for cryo-EM often contain a variety of structures. When such mixtures are subjected to single-particle analysis, the 2D projections of a number of 3D structures therefore need to be separated. A general solution to the mixture problem was provided first by 3D maximum-likelihood classification algorithms[25,26]. Because they incorporate a statistical description of the data, these methods are more robust to noise than those that were already in common use[27]. Alternative approaches to classification soon followed, which resulted in methods that turned the mixture problem into an opportunity. Whereas the presence of numerous structures previously blurred cryo-EM structures, valuable insight into protein dynamics could now be obtained from a single experiment[28].

When digital electron detectors became available commercially in 2013, the cryo-EM field was poised for a revolution. The unprecedented image quality that arose from these detectors enabled orientations to be assigned with greater accuracy. The ability to separate particles from distinct structural states was also improved. Structures that heralded this era include the coenzyme F_{420}-reducing hydrogenase[29], the mammalian ion channel transient receptor potential cation channel subfamily V member 1 (TRPV1) (ref. 30) and the large subunit of the mitochondrial ribosome in yeast[31]. The extension of maximum-likelihood methods into an empirical Bayesian approach made image processing more accessible to non-experts because crucial parameters no longer needed to be tuned; they were estimated from the data instead[32]. Moreover, the automated data-acquisition procedures that were developed originally for CCDs facilitated the recording of large datasets, from which the best particles could then be selected using image classification. As a result, in the past 3 years many research groups have solved cryo-EM structures to atomic resolution for a wide range of samples. Complexes with molecular weights of less than 200 kDa have become feasible targets for structure determination[33,34], and the achievable limits of resolution now extend to below 3 Å (refs 2, 35–37) and might even surpass 2 Å in favourable cases[34].

Opportunities for structure determination

Many of the newly determined structures represent proteins that are naturally embedded in membranes (Fig. 2). Such proteins are difficult to purify in solution because their hydrophobic membrane-spanning domains must be stabilized with detergents. Detergents also make crystallization notoriously difficult to achieve.

Consequently, membrane proteins are a blind spot for structural biology (Fig. 1), which is unfortunate because approximately half of all known small-molecule drugs bind to these proteins. However, structure determination through cryo-EM does not require crystallization. Instead, it is possible to image membrane proteins directly that have been solubilized in detergents or amphipols[38], or stabilized in a lipid environment using nanodiscs formed within the scaffold of an amphipathic protein belt[39] or the saposin–lipoprotein system[40]. The first membrane-protein structure to be solved using the new cryo-EM technology was TRPV1 (ref. 30). This protein is responsible for the burning sensation that chilli peppers impart and it is an important drug target for pain. Its structure was solved first in an empty state that had been solubilized in amphipols. A complex of TRPV1 with the spider toxin DkTx and a small molecule that is similar to capsaicin, the active component of chilli peppers, was also determined[41]. An improved TRPV1 structure that was determined in the more natural environment of a nanodisc enabled the visualization of lipid substrates and provided more detailed mechanistic insight into TRPV1 function[42]. After the initial TRPV1 structure was determined, the structures of many other medically relevant ion channels were published, including the voltage-dependent calcium channel $Ca_V1.1$ (ref. 43), a sodium–potassium channel[44] and the glycine receptor[45]. Together, these structures have yielded a wealth of information on how cells regulate ion transport across membranes.

Another advantage of cryo-EM is that flexible regions of proteins do not impede structure determination. To facilitate crystallization, flexible loops or sugars are typically removed using complicated protein-engineering approaches[46]. However, fully glycosylated wild-type proteins can be used for cryo-EM. For example, the structure of the human γ-secretase complex was solved despite it containing at least 11 sugar chains and a long disordered loop[33]. This membrane-embedded protease generates amyloid-β peptides that aggregate in the brains of people with Alzheimer's disease. With an ordered mass of about 130 kDa, human γ-secretase is the smallest cryo-EM structure to be determined at a resolution below 3.5 Å. Another example is the heavily glycosylated structure of the human immunodeficiency virus type 1 (HIV-1) envelope glycoprotein trimer. This protein recognizes receptors on the surface of immune cells and mediates the

BOX 1

Cryo-EM structure determination

Protein structure determination through cryo-EM involves several stages: sample grid preparation, data collection and data processing followed by 3D reconstruction (Box Fig.). A few microlitres of a purified protein solution are applied to a grid composed of a perforated carbon film and the excess liquid is blotted away. The grid is plunged into liquid ethane, which flash-freezes the sample and embeds the particles in vitreous ice. The grid is stored in liquid nitrogen until it is transferred to the transmission electron microscope. Two-dimensional images of proteins in various orientations within the grid's holes are then captured by the microscope's detector. The data are processed to combine images of the same protein into a 3D reconstruction of the protein's structure. The enzyme glutamate dehydrogenase[34] is presented as an example of a structure determined through cryo-EM.

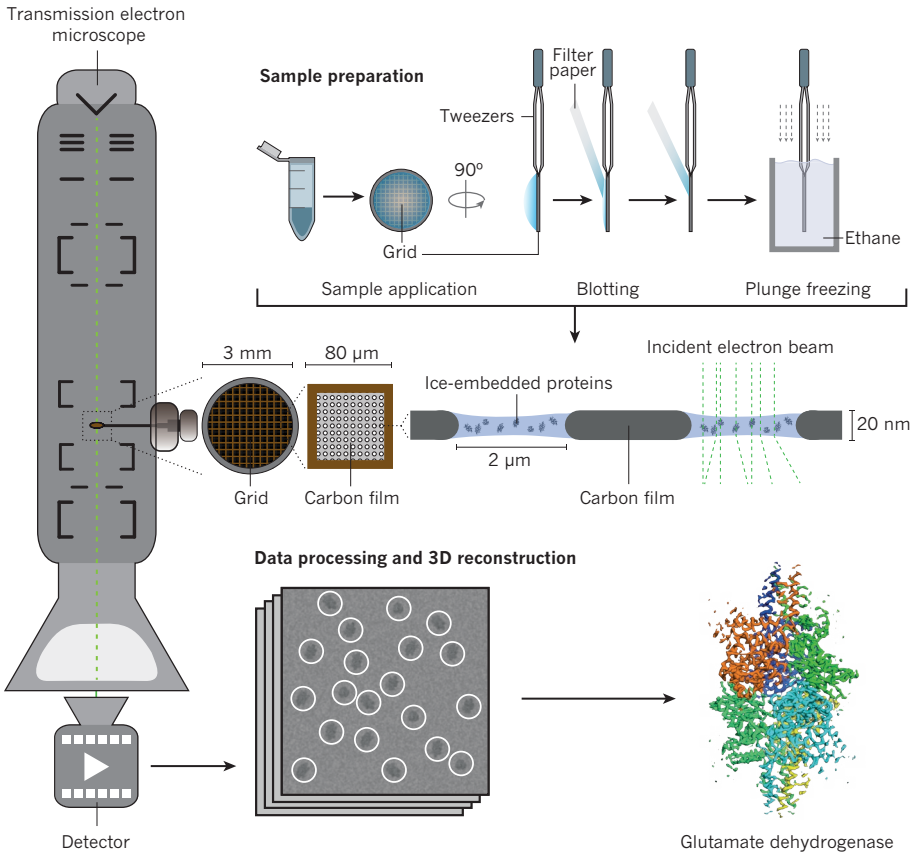

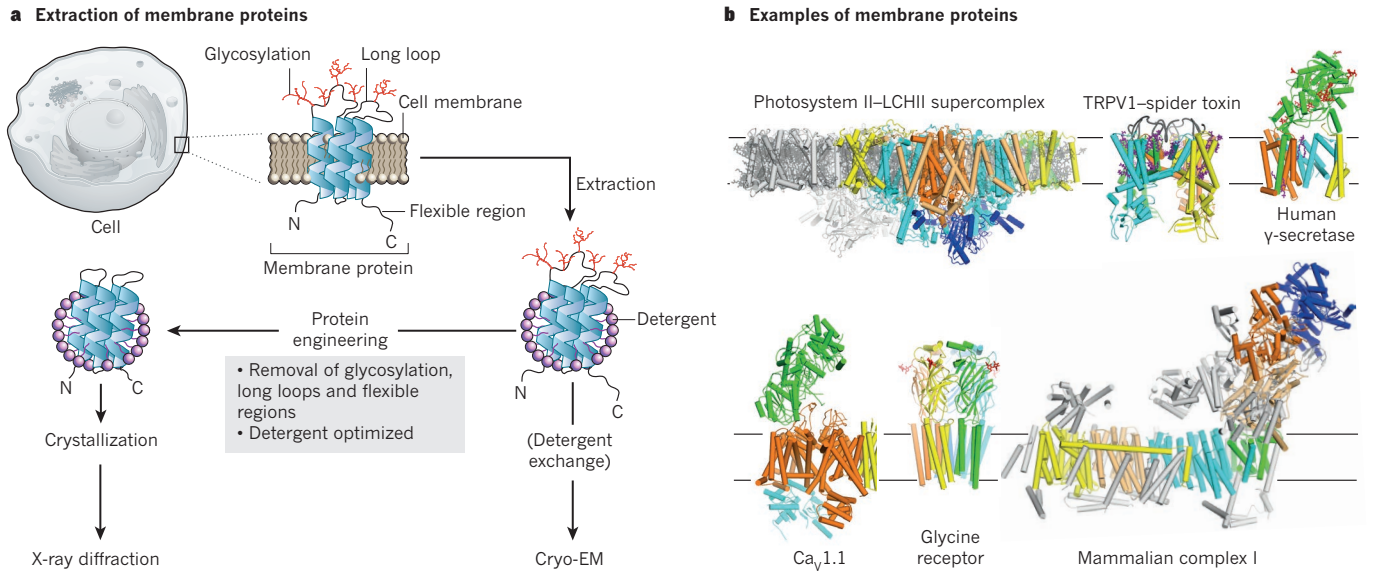

Figure 2 | Membrane protein structural biology. **a**, Proteins that are embedded in biological membranes must be extracted from the membrane using detergent solubilization techniques before their structures can be determined. The crystallization of membrane proteins for X-ray diffraction-based structure determination is difficult and often requires protein engineering to remove long loops, flexible regions and glycosylation. However, cryo-EM structure determination enables membrane proteins to be imaged directly in detergents or more natural environments such as nano-discs. The structures of glycosylated membrane proteins and very large membrane complexes can be determined through cryo-EM. **b**, Examples of membrane protein structures that were determined through cryo-EM: the photosystem II–light harvesting II supercomplex[60], TRPV1 in a complex with the spider toxin DxTx[42], human γ-secretase[33], the voltage-gated calcium channel Ca$_V$1.1 (ref. 43), the glycine receptor[45] and mammalian complex I (ref. 59) are shown as examples.

entry of HIV-1. Knowledge of the structure of the fully glycosylated native protein has provided important information that might help in the development of HIV-1 vaccines[47,48]. Similarly, the structures of Ebola virus glycoprotein GP1 bound to neutralizing antibodies[49] and to the transporter protein Niemann–Pick C1 (NPC1) (ref. 50) provide clues about immunity to Ebola in humans and how the virus fuses its membrane with that of the host.

Complexes that have been purified from native sources may also be suitable for cryo-EM-based structure determination. This is because wild-type proteins can be used and only micrograms of purified protein are required. Consequently, the structures of various large membrane-protein complexes that had resisted crystallographic studies have been determined, including the ryanodine receptor[51–53], the inositol triphosphate receptor[54], several glutamate receptors[55–58], mammalian complex I (ref. 59), photosystem II–light harvesting supercomplex (PSII–LHCII) (ref. 60) and ATP synthases[61,62].

The possibility of determining the structures of large complexes from native sources has also had a huge impact on the characterization of soluble macromolecular machines (Fig. 3). In the past 2 years, more than 50 high-resolution ribosome structures have been determined, which has yielded a wealth of information on the control of protein biosynthesis. For example, studies of both mammalian[63,64] and yeast[31] mitochondrial ribosomes have revealed how coevolution with the mitochondrial genome has affected their structures. Other macromolecular machines have also now become amenable to structural studies, as exemplified by the structures that have emerged of the inflammasome[65,66], the spliceosome[67–69], the signallosome[70,71], the exosome[72], the anaphase-promoting complex[73,73], the 26S proteasome[75,76], the SNARE (soluble NSF attachment protein receptor) complex[77,78], the dynein–dynactin complex[79,80], the chaperone heat shock protein 90 (ref. 81) and the serine/threonine protein kinase mTOR[82,83]. These all change conformation, rearrange their subunits and bind various partners and substrates during their assembly and working cycles. Cryo-EM enables the study of these often short-lived conformations and interactions, which are difficult to isolate or stabilize biochemically.

Nuclear complexes that act on DNA and RNA form another group of molecular machines that is difficult to analyse conventionally. Both the proteins and the oligonucleotide substrates in these complexes tend to be highly dynamic molecules that engage in transient interactions with each other. Consequently, it has proven challenging to make or purify many large nuclear complexes. In a showcase of the potential of cryo-EM for studying highly dynamic complexes, various cryo-EM-determined structures are starting to shed light on the molecular details of some of the most fundamental processes of life. For example, DNA replication machinery structures have unveiled some of the molecular details of how genomes are copied[84–87], and a number of structures of RNA polymerases have led to insight into how DNA is transcribed into RNA[88–92]. RNA polymerases have even been studied *in situ* by cryo-EM, inside the capsid of double-stranded RNA viruses[93,94]. Other examples of cryo-EM studies of nuclear complexes include: a structure that provides a fresh understanding of genetic recombination[95]; structures that show how the retroviral recombination machinery engages with the host nucleosome to insert its DNA[96,97]; a structure of the bacterial group II intron that reveals how this mobile DNA element catalyses self-splicing in conjunction with a small intron-encoded protein[98]; and structures that have aided our understanding of the mechanisms of type II and type III clustered regularly interspaced short palindromic repeat (CRISPR) systems[99,100].

In almost all of these studies, image classification played a crucial part in selecting structurally homogeneous subsets of particles for structure determination. For many structures, only a small fraction of the particles in the initial dataset is selected for use in the calculation of the final map. Most particles in cryo-EM datasets are unsuitable in some way for high-resolution structure determination and image classification enables only the best to be selected. Moreover, much like man-made machines, macromolecular machines make use of movements of parts relative to each other in their function. Whereas dynamic complexes would need to be trapped in a single state to facilitate crystallization, the new image classification algorithms offer the unique opportunity to visualize the full conformational freedom of such complexes in a single experiment (Fig. 4). A

striking example of this is the membrane-embedded ATP synthase, which acts as a molecular turbine, converting a proton flux into rotation to synthesize molecules of ATP, the energy currency of the cell. Image classification revealed the presence of three rotated states of the machine from a single cryo-EM dataset[61]. In another example, the imaging of actively translating human polysomes, which consist of multiple ribosomes bound to a single molecule of mRNA, followed by extensive image classification led to the production of structural snapshots of the entire translation cycle[101].

The future of cryo-EM

Several challenges must be overcome for cryo-EM-based structure determination to continue its transformative growth in structural biology. An immediate concern is the elevated cost of cryo-EM. High-resolution structure determination is best performed using 300 kV electron microscopes, which cost in excess of US$5 million and are accompanied by expensive maintenance contracts. Microscopes that operate at 200 kV are cheaper and can also be used to produce atomic-resolution structures[102,103]; but their cost is still on the order of millions of dollars. To facilitate broad access to high-end microscopes, regional or national cryo-EM facilities are quickly gaining in popularity[104]. However, the optimization of samples requires access to an electron microscope on a daily or weekly basis, which is not practical when using centralized facilities. In principle, expensive high-voltage machines are not needed for sample screening. But the cheaper microscopes that are available at present, which often operate at 100–120 kV, are unable to generate electrons that are all in-phase; they lack the coherence that is required to visualize particles with molecular weights below several hundreds of thousands of daltons. Consequently, there is an urgent need to develop affordable screening microscopes with more coherent electron sources.

The cost of storing and processing large volumes of data is also a problem. Automated data acquisition on a high-end microscope can yield several terabytes of images every day, and processing times can reach hundreds of thousands of computing core hours per dataset. To avoid the need to buy and maintain costly high-performance computing infrastructure, alternative solutions such as cloud computing[105] and the implementation of image-processing algorithms on cheaper graphics processing units (GPUs) are being explored[106,107].

As well as reducing costs and increasing the accessibility of high-end cryo-EM instruments, there is ample scope for improving the performance of microscope hardware. For example, progress has been achieved by increasing the efficiency of electron detection from about 30% when film is used to 50% for direct electron detectors. Such detectors could even be improved further. An important aspect of efficient electron detection is the ability to count individual electrons as they hit the detector, which requires fast read-outs[21,108]. Of the three commercially available detectors, at present only one is fast enough to enable counting; another needs to lower the intensity of the electron beam to avoid flooding the chip with too many events. The use of more modern technology, such as faster electronics and improved chip design, could enable the production of detectors with efficiencies of up to 90%.

Noise in images can be decreased further through the use of energy filters. These optical devices remove electrons that have lost part of their energy in the sample and can no longer contribute constructively to the image. Energy filters were originally considered to be most useful for thick samples such as whole cells, in which more electrons lose energy while passing through the sample. However, some of the highest resolution and smallest structures that are available were reconstructed from energy-filtered images, which indicates that the removal of these electrons is also beneficial for thinner samples[2,33,34,36].

Optical devices known as phase plates are another promising development for microscope hardware. They produce a difference in the phase of the scattered and the unscattered electron waves. This generates contrast that is improved by up to an order of magnitude in images at low resolution — of particular interest when imaging complexes that are too small to yield enough contrast with existing optics[109]. Aberration correctors, a further type of optical device, can yield better images, in particular at higher resolutions. These devices counteract the effects of imperfections in the optical system of the microscope through complicated combinations of lenses. Although not needed at present to reach resolutions of 3 Å or lower, such correctors might be helpful when higher resolutions of around 2 Å must be achieved[110].

The refinement of sample preparation methods provides another important opportunity for enhancing cryo-EM-based structure determination. Although movie processing has progressed enough to correct for beam-induced motion in samples, large movements of particles during the early stages of electron exposure are often too fast to be corrected[21,29,111]. This places a considerable constraint on the determination of structures at high resolution because most of the high-resolution information is destroyed by radiation damage during this early period[112]. Developments in sample preparation for cryo-EM aim to reduce or stop this motion, for example by replacing both the copper grid and the amorphous holey carbon film with gold[113], or by using films made of graphene or graphene oxide[114,115].

Requirements that concern the quantity and purity of samples can also be modified to boost cryo-EM outcomes. At present, several microlitres of a purified sample of protein, typically at a concentration of 0.1–5.0 µmol per litre, are needed to prepare a single cryo-EM grid. Purification of the sample on the grid itself, through the use of specifically adhered affinity tags[116], can relax demands on sample concentration and purity. And because less than 0.1% of the sample volume will remain on the grid after blotting, and only a fraction of the grid's surface is typically used for data acquisition, savings in sample volumes of multiple orders of magnitude are possible. Investigations that have pursued this direction include spraying picolitre-sized droplets of samples on cryo-EM grids[117]. Similar methods can

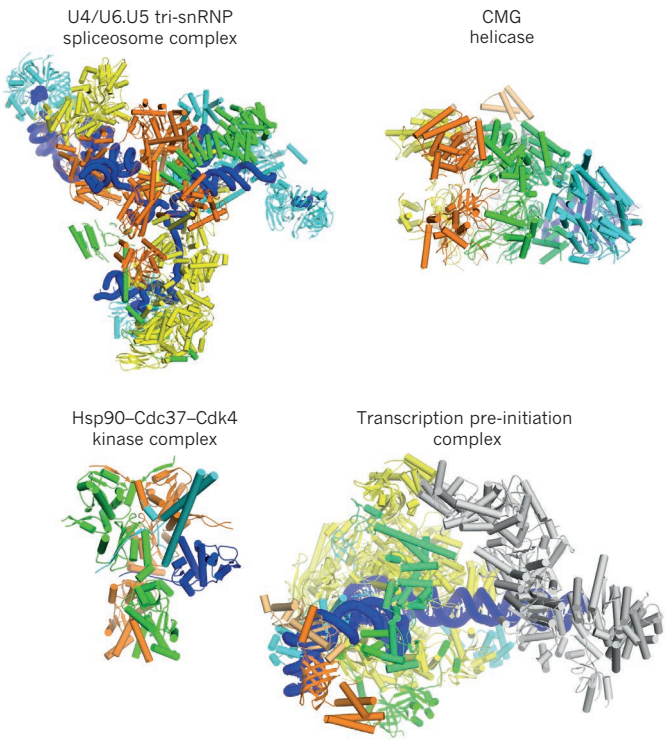

Figure 3 | Soluble macromolecular machines. Examples of cryo-EM structures are shown for the U4/U6.U5 tri-snRNP spliceosomal complex in yeast[67]; the eukaryotic replicative CMG helicase[86]; the human Hsp90–Cdc37–Cdk4 kinase complex[81]; and the human transcription pre-initiation complex[91].

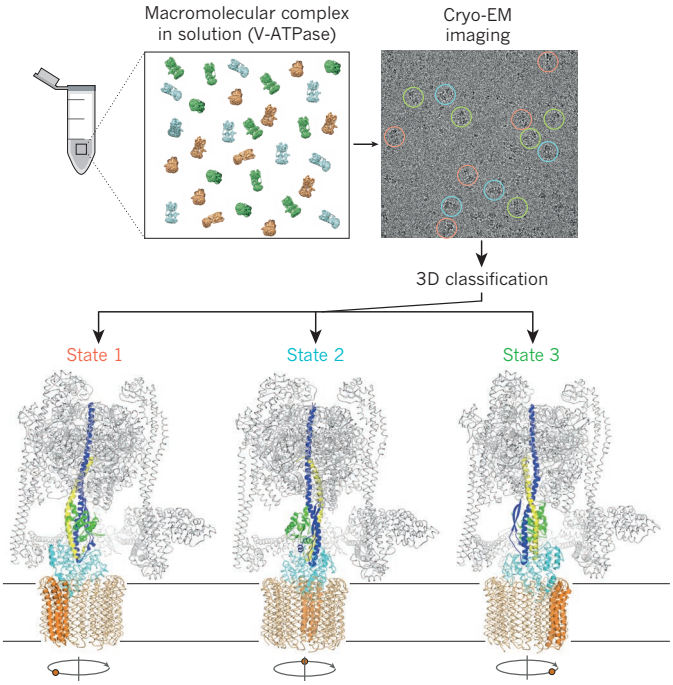

Figure 4 | Image classification enables the study of macromolecular dynamics. A mixture containing a macromolecular complex in distinct conformations or compositions (shown as red, blue and green objects) can be imaged directly using cryo-EM techniques. Three-dimensional image classification is then used to obtain structures for each state of the complex. Such classification therefore enables the functional cycles of dynamic molecular machines such as the eukaryotic V-ATPase[61] to be characterized from a single experiment.

be used in time-resolved studies in which multiple protein components are mixed together in a precisely timed manner[118]. When combined with modern microfluidic systems and the ability to tackle mixtures through image classification, this could enable reactions to be followed on a millisecond timescale[119].

In software development, superior image-formation models might be necessary to calculate structures of higher resolution. Improved image-processing algorithms are also needed to deal with complicated, multicomponent mixtures and to identify less common states. In particular, the presence of numerous continuously flexing domains still represents a challenge. Alternative procedures that describe the ensemble of structures in a dataset (instead of dividing the data into subsets) have the potential to reveal the conformational complexity of highly dynamic molecular machines[67,120].

Prospects

Each of the developments described in this Review has the potential to enlarge the scope of cryo-EM-based single-particle analysis and will lead to the collection of images with higher signal-to-noise ratios. Together with improved image-processing algorithms, such images will yield higher resolution structures of smaller complexes and of more complicated mixtures than is possible at present.

The ability to visualize proteins complexes with molecular weights of around 100 kDa will widen the applicability of the technique to many more drug targets. For example, G-protein-coupled receptors are sought-after targets for the pharmaceutical industry. In complex with conformation-specific antibodies or heterotrimeric G proteins, these receptors should become amenable to structure determination by cryo-EM. With the potential to achieve resolutions well beyond 3 Å (ref. 34) for complexes that are bound to drug candidates[121], cryo-EM structure-based drug design will become routine for targets that, at present, are extremely difficult to characterize using alternative techniques.

The ability to obtain structures from small subsets of the data through image processing, possibly in combination with sample preparation on the nanolitre scale, will also expand the applicability of cryo-EM to complexes with low abundance in the cell. Using time-resolved methods, even transient complexes and intermediate conformational states can be studied, providing unprecedented insight into the function of large macromolecular machines. For example, the structural characterization at the molecular (or even the atomic) level of extremely large and flexible machines such as the nuclear pore complex[122], as well as the characterization of complexes involved in the organization of chromatin[123], is now on the horizon.

Yet macromolecules do not act in isolation. The cell is densely packed with many molecules that interact to form highly intricate networks that are finely tuned to keep it alive. The detailed structural information about individual complexes that can be obtained through single-particle analysis needs to be understood in the context of the complexes' cellular environment. Excitingly, imaging with electrons could also provide unique opportunities in this task. For example, cryo-electron tomography can be used to build 3D reconstructions of frozen cells by taking multiple images of the same sample at different tilt angles inside the electron microscope[124]. Radiation damage is still a major limitation, but the resolution of the substructures that are repeated in the cell can be increased by applying averaging methods[125]. The tomographic approaches will benefit from the same developments in hardware and software that are driving forwards cryo-EM-based single-particle analysis. These techniques could bridge the gap between biophysics and cell biology and provide a road map for understanding of the cell at a molecular level. ■

Received 11 April; accepted 15 July 2016.

1. Alberts, B. The cell as a collection of protein machines: preparing the next generation of molecular biologists. *Cell* **92,** 291–294 (1998).
2. Banerjee, S. *et al.* 2.3 Å resolution cryo-EM structure of human p97 and mechanism of allosteric inhibition. *Science* **351,** 871–875 (2016).
3. Kühlbrandt, W. The resolution revolution. *Science* **343,** 1443–1444 (2014).
4. Taylor, K. A. & Glaeser, R. M. Electron diffraction of frozen, hydrated protein crystals. *Science* **186,** 1036–1037 (1974).
5. Dubochet, J., Chang, J.-J., Freeman, R., Lepault, J. & McDowall, A. W. Frozen aqueous suspensions. *Ultramicroscopy* **10,** 55–62 (1982).
6. Frank, J., Verschoor, A. & Boublik, M. Computer averaging of electron micrographs of 40S ribosomal subunits. *Science* **214,** 1353–1355 (1981).
7. Jiang, W. *et al.* Backbone structure of the infectious ε15 virus capsid revealed by electron cryomicroscopy. *Nature* **451,** 1130–1134 (2008).
8. Yu, X., Jin, L. & Zhou, Z. H. 3.88Å structure of cytoplasmic polyhedrosis virus by cryo-electron microscopy. *Nature* **453,** 415–419 (2008).
9. Zhang, X. *et al.* Near-atomic resolution using electron cryomicroscopy and single-particle reconstruction. *Proc. Natl Acad. Sci. USA* **105,** 1867–1872 (2008).
10. Villa, E. *et al.* Ribosome-induced changes in elongation factor Tu conformation control GTP hydrolysis. *Proc. Natl Acad. Sci. USA* **106,** 1063–1068 (2009).
11. Schuette, J.-C. *et al.* GTPase activation of elongation factor EF-Tu by the ribosome during decoding. *EMBO J.* **28,** 755–765 (2009).
12. Seidelt, B. *et al.* Structural insight into nascent polypeptide chain-mediated translational stalling. *Science* **326,** 1412–1415 (2009).
13. Agard, D., Cheng, Y., Glaeser, R. M. & Subramaniam, S. in *Advances in Imaging and Electron Physics* Vol. 185 (ed. Hawkes, P. W.) Ch. 2, 113–137 (Elsevier, 2014).
14. Frank, J. Generalized single-particle cryo-EM—a historical perspective. *Microscopy* **65,** 3–8 (2016).
15. Vinothkumar, K. R. & Henderson, R. Single particle electron cryomicroscopy: trends, issues and future perspective. *Q. Rev. Biophys.* **49,** e13 (2016).
16. Henderson, R. The potential and limitations of neutrons, electrons and X-rays for atomic resolution microscopy of unstained biological molecules. *Q. Rev. Biophys.* **28,** 171–193 (1995).
17. Krivanek, O. L. & Mooney, P. E. Applications of slow-scan CCD cameras in transmission electron microscopy. *Ultramicroscopy* **49,** 95–108 (1993).
18. Potter, C. S. *et al.* Leginon: a system for fully automated acquisition of 1000 electron micrographs a day. *Ultramicroscopy* **77,** 153–161 (1999).
19. McMullan, G., Chen, S., Henderson, R. & Faruqi, A. R. Detective quantum efficiency of electron area detectors in electron microscopy. *Ultramicroscopy* **109,** 1126–1143 (2009).
20. McMullan, G., Faruqi, A. R., Clare, D. & Henderson, R. Comparison of optimal performance at 300keV of three direct electron detectors for use in low dose electron microscopy. *Ultramicroscopy* **147,** 156–163 (2014).
A comparison of the three commercially available direct electron detectors; all were shown to perform better than photographic film.

21. Li, X. *et al.* Electron counting and beam-induced motion correction enable near-atomic-resolution single-particle cryo-EM. *Nature Methods* **10,** 584–590 (2013).
22. Brilot, A. F. *et al.* Beam-induced motion of vitrified specimen on holey carbon film. *J. Struct. Biol.* **177,** 630–637 (2012).
23. Campbell, M. G. *et al.* Movies of ice-embedded particles enhance resolution in electron cryo-microscopy. *Structure* **20,** 1823–1828 (2012).
24. Bai, X.-C., Fernandez, I. S., McMullan, G. & Scheres, S. H. W. Ribosome structures to near-atomic resolution from thirty thousand cryo-EM particles. *eLife* **2,** e00461 (2013).
25. Scheres, S. H. W. *et al.* Disentangling conformational states of macromolecules in 3D-EM through likelihood optimization. *Nature Methods* **4,** 27–29 (2007).
26. Lyumkis, D., Brilot, A. F., Theobald, D. L. & Grigorieff, N. Likelihood-based classification of cryo-EM images using FREALIGN. *J. Struct. Biol.* **183,** 377–388 (2013).
27. Sigworth, F. J. A. Maximum-likelihood approach to single-particle image refinement. *J. Struct. Biol.* **122,** 328–339 (1998).
28. Clare, D. K. *et al.* ATP-triggered conformational changes delineate substrate-binding and -folding mechanics of the GroEL chaperonin. *Cell* **149,** 113–123 (2012).
29. Allegretti, M., Mills, D. J., McMullan, G., Kühlbrandt, W. & Vonck, J. Atomic model of the F_{420}-reducing [NiFe] hydrogenase by electron cryo-microscopy using a direct electron detector. *eLife* **3,** e01963 (2014).
Refs 29–31 each present one of the first three high-resolution structures that heralded the resolution revolution in cryo-EM-based structure determination.
30. Liao, M., Cao, E., Julius, D. & Cheng, Y. Structure of the TRPV1 ion channel determined by electron cryo-microscopy. *Nature* **504,** 107–112 (2013).
31. Amunts, A. *et al.* Structure of the yeast mitochondrial large ribosomal subunit. *Science* **343,** 1485–1489 (2014).
32. Scheres, S. H. W. A Bayesian view on cryo-EM structure determination. *J. Mol. Biol.* **415,** 406–418 (2012).
A statistical framework for the classification and high-resolution refinement of cryo-EM structures that reduces the need for expert supervision.
33. Bai, X.-C. *et al.* An atomic structure of human γ-secretase. *Nature* **525,** 212–217 (2015).
34. Merk, A. *et al.* Breaking cryo-EM resolution barriers to facilitate drug discovery. *Cell* **165,** 1698–1707 (2016).
The highest reported resolution (1.8 Å) of a single-particle reconstruction, at present.
35. Campbell, M. G., Veesler, D., Cheng, A., Potter, C. S. & Carragher, B. 2.8 Å resolution reconstruction of the *Thermoplasma acidophilum* 20S proteasome using cryo-electron microscopy. *eLife* **4,** e06380 (2015).
36. Bartesaghi, A. *et al.* 2.2 Å resolution cryo-EM structure of β-galactosidase in complex with a cell-permeant inhibitor. *Science* **348,** 1147–1151 (2015).
37. Grant, T. & Grigorieff, N. Measuring the optimal exposure for single particle cryo-EM using a 2.6 Å reconstruction of rotavirus VP6. *eLife* **4,** e06980 (2015).
38. Althoff, T., Mills, D. J., Popot, J. L. & Kühlbrandt, W. Arrangement of electron transport chain components in bovine mitochondrial supercomplex $I_1III_2IV_1$. *EMBO J.* **30,** 4652–4664 (2011).
39. Bayburt, T. H. & Sligar, S. G. Membrane protein assembly into nanodiscs. *FEBS Lett.* **584,** 1721–1727 (2010).
40. Frauenfeld, J. *et al.* A saposin-lipoprotein nanoparticle system for membrane proteins. *Nature Methods* **13,** 345–351 (2016).
41. Cao, E., Liao, M., Cheng, Y. & Julius, D. TRPV1 structures in distinct conformations reveal activation mechanisms. *Nature* **504,** 113–118 (2013).
42. Gao, Y., Cao, E., Julius, D. & Cheng, Y. TRPV1 structures in nanodiscs reveal mechanisms of ligand and lipid action. *Nature* **534,** 347–351 (2016).
43. Wu, J. *et al.* Structure of the voltage-gated calcium channel $Ca_v1.1$ complex. *Science* **350,** aad2395 (2015).
44. Hite, R. K. *et al.* Cryo-electron microscopy structure of the Slo2.2 Na^+-activated K^+ channel. *Nature* **527,** 198–203 (2015).
45. Du, J., Lü, W., Wu, S., Cheng, Y. & Gouaux, E. Glycine receptor mechanism elucidated by electron cryo-microscopy. *Nature* **526,** 224–229 (2015).
46. Baker, M. Making membrane proteins for structures: a trillion tiny tweaks. *Nature Methods* **7,** 429–434 (2010).
47. Lyumkis, D. *et al.* Cryo-EM structure of a fully glycosylated soluble cleaved HIV-1 envelope trimer. *Science* **342,** 1484–1490 (2013).
48. Lee, J. H., Ozorowski, G. & Ward, A. B. Cryo-EM structure of a native, fully glycosylated, cleaved HIV-1 envelope trimer. *Science* **351,** 1043–1048 (2016).
49. Misasi, J. *et al.* Structural and molecular basis for Ebola virus neutralization by protective human antibodies. *Science* **351,** 1343–1346 (2016).
50. Gong, X. *et al.* Structural insights into the Niemann–Pick C1 (NPC1)-mediated cholesterol transfer and Ebola infection. *Cell* **165,** 1467–1478 (2016).
51. Yan, Z. *et al.* Structure of the rabbit ryanodine receptor RyR1 at near-atomic resolution. *Nature* **517,** 50–55 (2015).
52. Efremov, R. G., Leitner, A., Aebersold, R. & Raunser, S. Architecture and conformational switch mechanism of the ryanodine receptor. *Nature* **517,** 39–43 (2015).
53. Zalk, R. *et al.* Structure of a mammalian ryanodine receptor. *Nature* **517,** 44–49 (2015).
54. Fan, G. *et al.* Gating machinery of $InsP_3R$ channels revealed by electron cryomicroscopy. *Nature* **527,** 336–341 (2015).
55. Tajima, N. *et al.* Activation of NMDA receptors and the mechanism of inhibition by ifenprodil. *Nature* **534,** 63–68 (2016).
56. Zhu, S. *et al.* Mechanism of NMDA receptor inhibition and activation. *Cell* **165,** 704–714 (2016).
57. Herguedas, B. *et al.* Structure and organization of heteromeric AMPA-type glutamate receptors. *Science* **352,** aad3873 (2016).
58. Meyerson, J. R. *et al.* Structural mechanism of glutamate receptor activation and desensitization. *Nature* **514,** 328–334 (2014).
59. Vinothkumar, K. R., Zhu, J. & Hirst, J. Architecture of mammalian respiratory complex I. *Nature* **515,** 80–84 (2014).
60. Wei, X. *et al.* Structure of spinach photosystem II–LHCII supercomplex at 3.2 Å resolution. *Nature* **534,** 69–74 (2016).
61. Zhao, J., Benlekbir, S. & Rubinstein, J. L. Electron cryomicroscopy observation of rotational states in a eukaryotic V-ATPase. *Nature* **521,** 241–245 (2015).
An example of how image classification can reveal numerous functional states of dynamic molecular machines from a single experiment.
62. Allegretti, M. *et al.* Horizontal membrane-intrinsic α-helices in the stator a-subunit of an F-type ATP synthase. *Nature* **521,** 237–240 (2015).
63. Amunts, A., Brown, A., Toots, J., Scheres, S. H. W. & Ramakrishnan, V. The structure of the human mitochondrial ribosome. *Science* **348,** 95–98 (2015).
64. Greber, B. J. *et al.* The complete structure of the 55S mammalian mitochondrial ribosome. *Science* **348,** 303–308 (2015).
65. Zhang, L. *et al.* Cryo-EM structure of the activated NAIP2-NLRC4 inflammasome reveals nucleated polymerization. *Science* **350,** 404–409 (2015).
66. Hu, Z. *et al.* Structural and biochemical basis for induced self-propagation of NLRC4. *Science* **350,** 399–404 (2015).
67. Nguyen, T. H. D. *et al.* Cryo-EM structure of the yeast U4/U6.U5 tri-snRNP at 3.7 Å resolution. *Nature* **530,** 298–302 (2016).
68. Agafonov, D. E. *et al.* Molecular architecture of the human U4/U6.U5 tri-snRNP. *Science* **351,** 1416–1420 (2016).
69. Wan, R. *et al.* The 3.8 Å structure of the U4/U6.U5 tri-snRNP: insights into spliceosome assembly and catalysis. *Science* **351,** 466–475 (2016).
70. Mosadeghi, R. *et al.* Structural and kinetic analysis of the COP9–signalosome activation and the cullin–RING ubiquitin ligase deneddylation cycle. *eLife* **5,** e12102 (2016).
71. Cavadini, S. *et al.* Cullin–RING ubiquitin E3 ligase regulation by the COP9 signalosome. *Nature* **531,** 598–603 (2016).
72. Liu, J.-J. *et al.* CryoEM structure of yeast cytoplasmic exosome complex. *Cell Res.* **26,** 822–837 (2016).
73. Chang, L., Zhang, Z., Yang, J., McLaughlin, S. H. & Barford, D. Atomic structure of the APC/C and its mechanism of protein ubiquitination. *Nature* **522,** 450–454 (2015).
74. Zhang, S. *et al.* Molecular mechanism of APC/C activation by mitotic phosphorylation. *Nature* **533,** 260–264 (2016).
75. Schweitzer, A. *et al.* Structure of the human 26S proteasome at a resolution of 3.9 Å. *Proc. Natl Acad. Sci. USA* **113,** 7816–7821 (2016).
76. Dambacher, C. M., Worden, E. J., Herzik, M. A., Martin, A. & Lander, G. C. Atomic structure of the 26S proteasome lid reveals the mechanism of deubiquitinase inhibition. *eLife* **5,** e13027 (2016).
77. Zhou, Q. *et al.* Cryo-EM structure of SNAP-SNARE assembly in 20S particle. *Cell Res.* **25,** 551–560 (2015).
78. Zhao, M. *et al.* Mechanistic insights into the recycling machine of the SNARE complex. *Nature* **518,** 61–67 (2015).
79. Chowdhury, S., Ketcham, S. A., Schroer, T. A. & Lander, G. C. Structural organization of the dynein–dynactin complex bound to microtubules. *Nature Struct. Mol. Biol.* **22,** 345–347 (2015).
80. Urnavicius, L. *et al.* The structure of the dynactin complex and its interaction with dynein. *Science* **347,** 1441–1446 (2015).
81. Verba, K. A. *et al.* Atomic structure of Hsp90-Cdc37-Cdk4 reveals that Hsp90 traps and stabilizes an unfolded kinase. *Science* **352,** 1542–1547 (2016).
82. Aylett, C. H. S. *et al.* Architecture of human mTOR complex 1. *Science* **351,** 48–52 (2016).
83. Baretić, D., Berndt, A., Ohashi, Y., Johnson, C. M. & Williams, R. L. Tor forms a dimer through an N-terminal helical solenoid with a complex topology. *Nature Commun.* **7,** 11016 (2016).
84. Fernández-Leiro, R., Conrad, J., Scheres, S. H. & Lamers, M. H. Cryo-EM structures of the *E. coli* replicative DNA polymerase reveal its dynamic interactions with the DNA sliding clamp, exonuclease and τ. *eLife* **4,** e11134 (2015).
85. Li, N. *et al.* Structure of the eukaryotic MCM complex at 3.8 Å. *Nature* **524,** 186–191 (2015).
86. Yuan, Z. *et al.* Structure of the eukaryotic replicative CMG helicase suggests a pumpjack motion for translocation. *Nature Struct. Mol. Biol.* **23,** 217–224 (2016).
87. Abid Ali, F. *et al.* Cryo-EM structures of the eukaryotic replicative helicase bound to a translocation substrate. *Nature Commun.* **7,** 10708 (2016).
88. Hoffmann, N. A. *et al.* Molecular structures of unbound and transcribing RNA polymerase III. *Nature* **528,** 231–236 (2015).
89. Murakami, K. *et al.* Structure of an RNA polymerase II preinitiation complex. *Proc. Natl Acad. Sci. USA* **112,** 13543–13548 (2015).
90. Bernecky, C., Herzog, F., Baumeister, W., Plitzko, J. M. & Cramer, P. Structure of transcribing mammalian RNA polymerase II. *Nature* **529,** 551–554 (2016).
91. He, Y. *et al.* Near-atomic resolution visualization of human transcription promoter opening. *Nature* **533,** 359–365 (2016).
92. Plaschka, C. *et al.* Transcription initiation complex structures elucidate DNA opening. *Nature* **533,** 353–358 (2016).
93. Zhang, X. *et al. In situ* structures of the segmented genome and RNA polymerase complex inside a dsRNA virus. *Nature* **527,** 531–534 (2015).
94. Liu, H. & Cheng, L. Cryo-EM shows the polymerase structures and a nonspooled genome within a dsRNA virus. *Science* **349,** 1347–1350 (2015).

95. Ru, H. *et al.* Molecular mechanism of V(D)J recombination from synaptic RAG1–RAG2 complex structures. *Cell* **163,** 1138–1152 (2015); erratum **163,** 1807 (2015).
96. Maskell, D. P. *et al.* Structural basis for retroviral integration into nucleosomes. *Nature* **523,** 366–369 (2015).
97. Ballandras-Colas, A. *et al.* Cryo-EM reveals a novel octameric integrase structure for betaretroviral intasome function. *Nature* **530,** 358–361 (2016).
98. Qu, G. *et al.* Structure of a group II intron in complex with its reverse transcriptase. *Nature Struct. Mol. Biol.* **23,** 549–557 (2016).
99. Jiang, F. *et al.* Structures of a CRISPR–Cas9 R-loop complex primed for DNA cleavage. *Science* **351,** 867–871 (2016).
100. Taylor, D. W. *et al.* Structures of the CRISPR–Cmr complex reveal mode of RNA target positioning. *Science* **348,** 581–585 (2015).
101. Behrmann, E. *et al.* Structural snapshots of actively translating human ribosomes. *Cell* **161,** 845–857 (2015).
102. Campbell, M. G. *et al.* Near-atomic resolution reconstructions using a mid-range electron microscope operated at 200kV. *J. Struct. Biol.* **188,** 183–187 (2014).
103. Liang, B. *et al.* Structure of the L protein of vesicular stomatitis virus from electron cryomicroscopy. *Cell* **162,** 314–327 (2015).
104. Saibil, H. R., Grünewald, K. & Stuart, D. I. A national facility for biological cryo-electron microscopy. *Acta Crystallogr. D* **71,** 127–135 (2015).
105. Cianfrocco, M. A. & Leschziner, A. E. Low cost, high performance processing of single particle cryo-electron microscopy data in the cloud. *eLife* **4,** e06664 (2015).
106. Schmeisser, M. *et al.* Parallel, distributed and GPU computing technologies in single-particle electron microscopy. *Acta Crystallogr. D* **65,** 659–671 (2009).
107. Kimanius, D., Forsberg, B. O., Scheres, S. & Lindahl, E. Accelerated cryo-EM structure determination with parallelisation using GPUs in RELION-2. Preprint at http://dx.doi.org/10.1101/059717 (2016).
108. McMullan, G., Clark, A. T., Turchetta, R. & Faruqi, A. R. Enhanced imaging in low dose electron microscopy using electron counting. *Ultramicroscopy* **109,** 1411–1416 (2009).
109. Danev, R. & Baumeister, W. Cryo-EM single particle analysis with the Volta phase plate. *eLife* **5,** e13046 (2016).
110. Fischer, N. *et al.* Structure of the *E. coli* ribosome–EF-Tu complex at <3 Å resolution by Cs-corrected cryo-EM. *Nature* **520,** 567–570 (2015).
111. Scheres, S. H. Beam-induced motion correction for sub-megadalton cryo-EM particles. *eLife* **3,** e03665 (2014).
112. Stark, H., Zemlin, F. & Boettcher, C. Electron radiation damage to protein crystals of bacteriorhodopsin at different temperatures. *Ultramicroscopy* **63,** 75–79 (1996).
113. Russo, C. J. & Passmore, L. A. Ultrastable gold substrates for electron cryomicroscopy. *Science* **346,** 1377–1380 (2014).
114. Russo, C. J. & Passmore, L. A. Controlling protein adsorption on graphene for cryo-EM using low-energy hydrogen plasmas. *Nature Methods* **11,** 649–652 (2014).
115. Pantelic, R. S., Meyer, J. C., Kaiser, U., Baumeister, W. & Plitzko, J. M. Graphene oxide: a substrate for optimizing preparations of frozen-hydrated samples. *J. Struct. Biol.* **170,** 152–156 (2010).
116. Kelly, D. F., Dukovski, D. & Walz, T. New applications for affinity grids in preparing EM specimens. *Microsc. Microanal.* **16** (suppl. S2), 840–841 (2010).
117. Jain, T., Sheehan, P., Crum, J., Carragher, B. & Potter, C. S. Spotiton: a prototype for an integrated inkjet dispense and vitrification system for cryo-TEM. *J. Struct. Biol.* **179,** 68–75 (2012).
118. Unwin, N. Acetylcholine receptor channel imaged in the open state. *Nature* **373,** 37–43 (1995).
119. Chen, B. *et al.* Structural dynamics of ribosome subunit association studied by mixing-spraying time-resolved cryogenic electron microscopy. *Structure* **23,** 1097–1105 (2015).
120. Dashti, A. *et al.* Trajectories of the ribosome as a Brownian nanomachine. *Proc. Natl Acad. Sci. USA* **111,** 17492–17497 (2014).
121. Li, H. *et al.* Structure- and function-based design of *Plasmodium*-selective proteasome inhibitors. *Nature* **530,** 233–236 (2016).
122. Kosinski, J. *et al.* Molecular architecture of the inner ring scaffold of the human nuclear pore complex. *Science* **352,** 363–365 (2016).
123. Song, F. *et al.* Cryo-EM study of the chromatin fiber reveals a double helix twisted by tetranucleosomal units. *Science* **344,** 376–380 (2014).
124. Baumeister, W. Electron tomography: towards visualizing the molecular organization of the cytoplasm. *Curr. Opin. Struct. Biol.* **12,** 679–684 (2002).
125. Mahamid, J. *et al.* Visualizing the molecular sociology at the HeLa cell nuclear periphery. *Science* **351,** 969–972 (2016).
This work presents an exciting vision of how cryo-electron tomography and sub-tomogram averaging can bridge the gap between the structural biology of isolated complexes and cell biology.

Acknowledgements We thank Y. Cheng, D. Barford and R. Henderson for comments on an early version of this manuscript. S.H.W.S is funded by the UK Medical Research Council (MC_UP_A025_1013).

Author Information Reprints and permissions information is available at www.nature.com/reprints. The authors declare no competing financial interests. Readers are welcome to comment on the online version of this paper at go.nature.com/2bqncxm. Correspondence should be addressed to S.H.W.S. (scheres@mrc-lmb.cam.ac.uk).